ISSN 1674-1056
http://cpb.iphy.ac.cn
http://iopscience.iop.org/cpb
中国物理 B
Chinese Physics
中国物理
Chinese Physics B

Formation of electron depletion layer and parallel electric field in the separatrix region of anti-parallel magnetic reconnection

Zisheng Li(李子圣), Huanyu Wang(王焕宇), Xinliang Gao(高新亮)

Citation: Chin. Phys. B . 2019, 28(7): 075203. **doi:** 10.1088/1674-1056/28/7/075203
Journal homepage: http://cpb.iphy.ac.cn; http://iopscience.iop.org/cpb

What follows is a list of articles you may be interested in

UAV flight test of plasma slats and ailerons with microsecond dielectric barrier discharge

Zhi Su(苏志), Jun Li(李军), Hua Liang(梁华), Bo-Rui Zheng(郑博睿), Biao Wei(魏彪), Jie Chen(陈杰), Li-Ke Xie(谢理科)
Chin. Phys. B . 2018, 27(10): 105205. **doi:** 10.1088/1674-1056/27/10/105205

Toroidal rotation induced by 4.6 GHz lower hybrid current drive on EAST tokamak

Xiang-Hui Yin(尹相辉), Jun Chen(陈俊), Rui-Ji Hu(胡睿佶), Ying-Ying Li(李颖颖), Fu-Di Wang(王福地), Jia Fu(符佳), Bo-Jiang Ding(丁伯江), Mao Wang(王茂), Fu-Kun Liu(刘甫坤), Qing Zang(臧庆), Yue-Jiang Shi(石跃江), Bo Lyu(吕波), Bao-Nian Wan(万宝年), EAST team
Chin. Phys. B . 2017, 26(11): 115203. **doi:** 10.1088/1674-1056/26/11/115203

Out-of-plane shear flow effects on fast magnetic reconnection in a two-dimensional hybrid simulation model

Wang Lin, Wang Xian-Qu, Wang Xiao-Gang, Liu Yue
Chin. Phys. B . 2014, 23(2): 025203. **doi:** 10.1088/1674-1056/23/2/025203

Numerical study on the electron-wall interaction in a Hall thruster with segmented electrodes placed at the channel exit

Qing Shao-Wei, E Peng, Duan Ping, Xu Dian-Guo
Chin. Phys. B . 2013, 22(8): 085203. **doi:** 10.1088/1674-1056/22/8/085203

Using short pulses to enhance the production rate of vibrationally excited hydrogen molecules in hydrogen discharge

Sun Ji-Zhong,Li Xian-Tao,Bai Jing,Wang De-Zhen
Chin. Phys. B . 2012, 21(5): 055205. **doi:** 10.1088/1674-1056/21/5/055205

Formation of electron depletion layer and parallel electric field in the separatrix region of anti-parallel magnetic reconnection*

Zisheng Li(李子圣)[1,2], Huanyu Wang(王焕宇)[1,2,†], and Xinliang Gao(高新亮)[1,2]

[1] CAS Key Laboratory of Geospace Environment, School of Earth and Space Sciences, University of Science and Technology of China, Hefei 230026, China

[2] CAS Center for Excellence in Comparative Planetology, Hefei 230026, China

(Received 16 January 2019; revised manuscript received 12 April 2019; published online 11 June 2019)

It is generally accepted that during collisionless magnetic reconnection, electrons flow toward the X line in the separatrix region, and then an electron depletion layer is formed. In this paper, with two-dimensional (2D) particle-in-cell (PIC) simulation, we investigate the characteristics of the separatrix region during magnetic reconnection. In addition to the electron depletion layer, we find that there still exists an electric field parallel to the magnetic field in the separatrix region. Because a reduced ion-to-electron mass ratio and light speed are usually used in PIC simulation models, we also change these parameters to analyze the characteristics of the separatrix region. It is found that the increase in the ion-to-electron mass ratio makes the electron depletion layer and the parallel electric field more obvious, while the influence of light speed is less pronounced.

Keywords: magnetic reconnection, separatrix region, electron depletion layer

PACS: 52.35.Vd, 52.65.Rr, 52.30.–q **DOI:** 10.1088/1674-1056/28/7/075203

1. Introduction

During the topological rearrangement of magnetic field lines occurring in the magnetic reconnection, in addition to the well-known dissipation from magnetic energy into plasma kinetic energy,[1–6] the production of superthermal electrons is also an important ingredient.[7–16] The reconnection electric field in the vicinity of the X line was considered to be the only site to account for electron acceleration during magnetic reconnection until the existence of the parallel electric field was revealed by Wang *et al.* with cluster observation.[17] Recently, the characteristics of the separatrix region have been gaining more and more attention.[18–24]

The separatrix region separates the ion diffusion region into the inflow and outflow regions. The ions flow toward the X line in the inflow region and move away from the X line in the outflow region.[25,26] However, because the electrons are frozen in the magnetic field while the ions are unmagnetized, the electron motions are different from those of ions.[18,26,27] The electrons move toward the X line in the separatrix region, and are then accelerated by the inductive electric field near the X line; at last, they are directed away along the magnetic field in the region, which is closer to the center of the current sheet.[7–9] This current system leads to a quadrupole structure of the Hall magnetic field (perpendicular to the reconnection plane).[25–33] At the same time, an electron depletion region where the electron density is smaller than in the nearby regions is formed in the separatrix region, which results in a net positive charge therein and an electric field pointing to the center of the current sheet.[34–36] Recently, satellite observations revealed the existence of a parallel electric field in the separatrix region, which indicates that the separatrix region also plays an important role in electron acceleration.[17,37] In this paper, with two-dimensional (2D) particle-in-cell (PIC) simulations, we study the formation of the parallel electric field, as well as the electron depletion layer in the separatrix region. The influences of the ion-to-electron mass ratio and light speed are also investigated.

2. Simulation method

In our 2D PIC simulation model, the electromagnetic field defined on the grids are calculated by an explicit algorithm of Maxwell equations, and the movement of particles is governed by the Lorentz force. The particles can only move in the x–z plane, and their velocities have three components. The details of our simulation model can be found in Ref. [8], and the code has been widely used to study magnetic reconnection and plasma waves.[38–43] The initial configuration is a one-dimensional Harris current sheet in the reconnection plane (the x–z plane). The magnetic field and plasma density are given by the following equations:

$$\boldsymbol{B}_0(z) = B_0 \tanh\left(\frac{z}{\delta}\right)\boldsymbol{e}_x, \tag{1}$$

$$n(z) = n_\mathrm{b} + n_0 \operatorname{sech}^2\left(\frac{z}{\delta}\right), \tag{2}$$

*Project supported by the National Natural Science Foundation of China (Grant Nos. 41774169, 41527804, and 41804159), the Key Research Program of Frontier Sciences, Chinese Academy of Sciences (Grant No. QYZDJ-SSW-DQC010), and the Youth Innovation Promotion Association of the Chinese Academy of Sciences (Grant No. 2016395).

†Corresponding author. E-mail: iuwon@ustc.edu.cn

© 2019 Chinese Physical Society and IOP Publishing Ltd

where B_0 is the asymptotical magnetic field, n_b represents a uniform background plasma density, and n_0 is the peak value of the plasma density corresponding to the Harris current sheet. δ is the half width of the current sheet.

Table 1. Simulation parameters for runs 1–7.

Run	m_i/m_e	c/v_A	Ω_{pe}/Ω_{e0}
1	25	15	3
2	49	15	2.14
3	144	15	1.25
4	225	15	1
5	144	36	3
6	144	25.7	2.14
7	144	12	1

Both ion and electron distributions satisfy the Maxwell function, and their drift velocities along the y direction satisfy $V_{i0}/V_{e0} = -T_{e0}/T_{i0}$, where V_{i0} (V_{e0}) and T_{i0} (T_{e0}) represent the drift velocity and the initial temperature of ions (electrons), respectively. The simulation domain is $L_x \times L_z = 25.6d_i \times 12.8d_i$ (where $d_i = c/\Omega_{pi}$ is the ion inertial length based on n_0). The number of grids is 1024×512, and then the grid size is $\Delta x = \Delta z = 0.025d_i$. In our simulations, we choose $\delta = 0.5c/\Omega_{pi}$, $n_b = 0.2n_0$, $T_{i0}/T_{e0} = 1$, and the time step is $\Omega_{i0}\Delta t = 5.0 \times 10^{-3}$ (where Ω_{i0} is the ion gyrofrequency based on B_0). The ion-to-electron mass ratio m_i/m_e, the ratio of the light speed to the Alfvén speed c/v_A (where v_A is the Alfvén speed based on B_0 and n_0), and the corresponding Ω_{pe}/Ω_{e0} (where Ω_{pe} is the electron plasma frequency based on n_0) are listed in Table 1. The periodic boundary condition is used in the x direction; meanwhile, particles are reflected when they reach the boundary in the z direction and the conducting boundary condition is used for the electromagnetic field. More than 100 million particles are used in the simulations. Magnetic reconnection is initiated by a small flux perturbation.

3. Simulation results

We first describe the characteristics of the separatrix region in run 3. In run 3, the ion-to-electron mass ratio is $m_i/m_e = 144$, and the light speed is $c/v_A = 15$. Figure 1 plots the time evolution of the reconnected flux ψ for run 3. The reconnection electric field can be estimated by calculating the slope of the reconnection flux. From the figure, it is easy to find that the magnetic field lines begin to be reconnected at about $\Omega_{i0}t = 15$, and the reconnection rate (the reconnection electric field at the X line) attains the maximum value at about $\Omega_{i0}t = 17.2$.

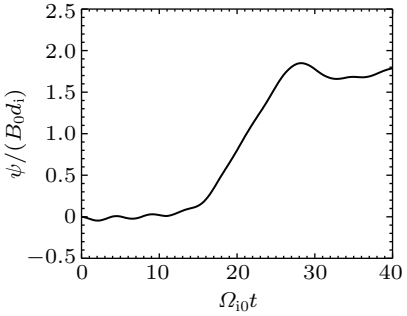


Fig. 1. The time evolution of the reconnected flux ψ for run 3.

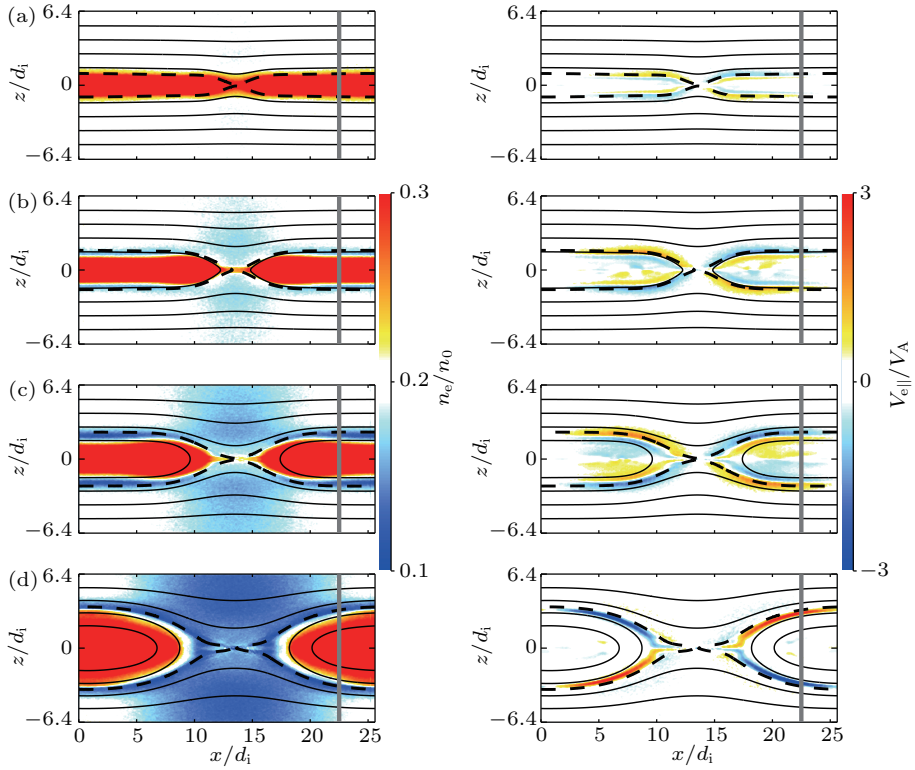


Fig. 2. The electron number density n_e (left panels) and parallel electron bulk velocity $V_{e\|}$ (right panels) for run 3 at $\Omega_{i0}t =$ (a) 15, (b) 17.5, (c) 20, and (d) 26.5. Magnetic field lines are shown by the black solid curves in the figure. The separatrices are indicated by the black dashed lines.

Figure 2 shows the electron number density n_e and parallel electron bulk velocity $V_{e\parallel}$ at $\Omega_{i0}t = 15$, 17.5, 20, and 26.5 for run 3. The magnetic field lines are also shown in the figure in order to more clearly display the evolution of the electron number density and parallel electron bulk velocity. With the occurrence of magnetic reconnection at about $\Omega_{i0}t = 15$, the electrons in the separatrix region flow toward the X line while they tend to be away from the X line along the magnetic field in the region, which is closer to the center of the current sheet. As demonstrated in Ref. [18], such an electron flow will result in an electron depletion layer in the separatrix region. Therefore, with the proceeding magnetic reconnection, an electron depletion layer is formed in the separatrix region at about $\Omega_{i0}t = 16$. After the reconnection rate attains the maximum value, the electron flow toward the X line begins to be weaker and weaker, and then disappears. However, the electron depletion layer can last for a much longer time.

The formation of the electron depletion layer can be exhibited more clearly in Fig. 3, which presents the electron number density n_e along the grey lines (at $x = 22.5d_i$ parallel to the z axis) denoted in the left panels of Fig. 2 at $\Omega_{i0}t = 15$, 17.5, 20, and 26.5 for run 3. In order to display these values more clearly, we only plot them from $z = 1.0d_i$ to $z = 6.0d_i$ along the denoted lines. The separatrix region will move away from the center of the current layer as the magnetic reconnection continues. After analyzing the difference between the electron number density n_e and the Gaussian fit for n_e, we can estimate the width of the electron depletion layer in the separatrix region as $1.2d_i$–$1.5d_i$. The minimum value of the electron density, which can be attained in the separatrix region at almost the same time as when the reconnection rate reaches the maximum value, is about $0.16n_0$.

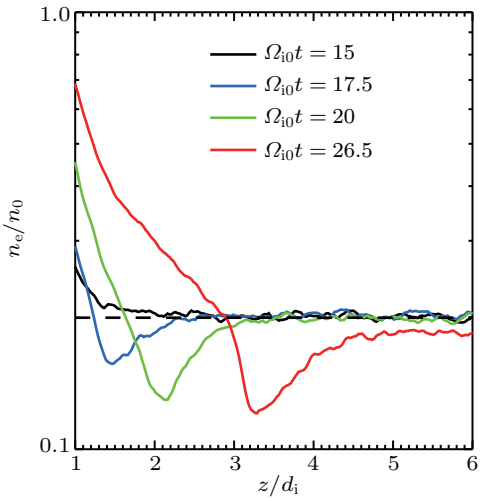


Fig. 3. The electron number density n_e along the grey lines denoted in the left panels of Fig. 2 at $\Omega_{i0}t = 15$ (black solid line), 17.5 (blue solid line), 20 (green solid line), and 26.5 (red solid line) for run 3. The initial electron density in the inflow region $n_b = 0.2n_0$ is indicated by the black dashed line in the figure.

Figure 4 shows the time evolution of the parallel electron bulk flow velocity $V_{e\parallel}$ along the grey lines denoted in the right panels of Fig. 2 for run 3. We only plot the profile of $V_{e\parallel}$ from $z = 0d_i$ to $z = 6.0d_i$ along the denoted lines. At $\Omega_{i0}t = 17.5$, the reconnection rate reaches the maximum value, and the parallel electron flow toward the X line also obtains a maximum value in the separatrix region, which is about $1.1v_A$. The maximum value of the parallel electron flow away from the X line occurs later at $\Omega_{i0}t = 26.5$, and is about $-3.2v_A$.

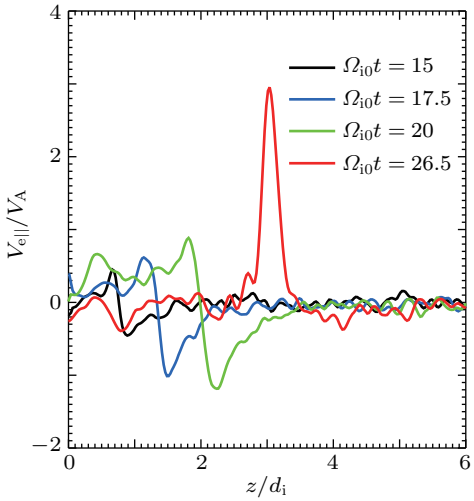


Fig. 4. The parallel electron bulk flow velocity $V_{e\parallel}$ along the grey lines denoted in the right panels of Fig. 2 at $\Omega_{i0}t = 15$ (black solid line), 17.5 (blue solid line), 20 (green solid line), and 26.5 (red solid line) for run 3.

Figures 5(a) and 5(b) respectively describe the parallel electric field $E_\parallel$ and the parallel electrostatic potential $\Phi_\parallel$ along the separatrix in the first quadrant at $\Omega_{i0}t = 15$, 17.5, 20, and 26.5 for run 3. Here, the electrostatic potential is defined as $\Phi_\parallel(l) = \int_X^l E_\parallel \mathrm{d}l$, which is integrated along the separatrix in the first quadrant from the X line. Please note that the gradient of $\Phi_\parallel$ perpendicular to the magnetic field has physical significance, and $\Phi_\parallel$ is only a pseudo-potential that measures the work done by the electric field as an electron moves along the magnetic field line. Obviously, there exists the parallel electric field along the separatrix. At $\Omega_{i0}t = 15$, the parallel electric field points away from the X line, and its amplitude becomes large as magnetic reconnection continues until the reconnection rate decreases. However, from about $\Omega_{i0}t = 17$, the parallel electric field pointing toward the X line is developed near the X line. The electron flow can be accelerated in the direction along the separatrix toward the X line by the positive parallel electric field. However, in the vicinity of the X line, the negative parallel electric field, which points toward the X line, will block the electron inflow.

The spatial distributions of net charge in the simulation domain for run 3, measured by $(n_i - n_e)/n_0$, are shown in Figs. 6(a) and 6(b) at $\Omega_{i0}t = 17.5$ and 20, respectively. It can be found that the net charge is positive in the separatrix region, which is caused by the depletion of the electron density.

However, we can find that in the pileup region the net charge begins to be negative after the reconnection rate reaches the maximum value, and it is formed when the accelerated electrons from the X line are blocked. Such distribution of the net charge results in the parallel electric field described in Fig. 5.

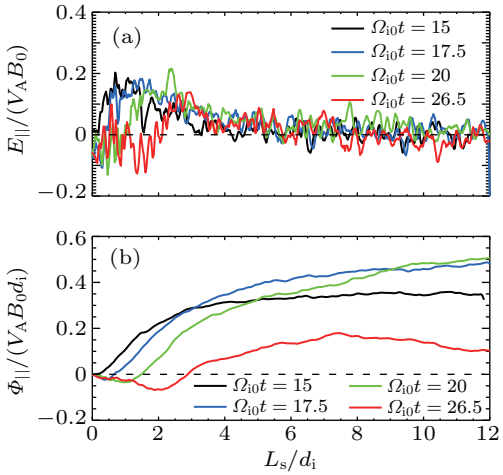


Fig. 5. The profiles of (a) the parallel electric field $E_\parallel$ and (b) the parallel electrostatic potential $\Phi_\parallel$ along the separatrix in the first quadrant at $\Omega_{i0}t = 15$ (black solid lines), 17.5 (blue solid lines), 20 (green solid lines), and 26.5 (red solid lines) for run 3. In the figure, the distance L_s is measured from the X line along the upper-right separatrix.

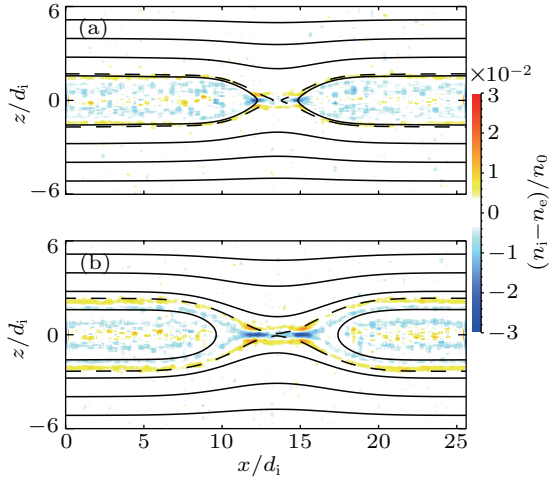


Fig. 6. The spatial distribution of net charge in the simulation domain for run 3 at (a) $\Omega_{i0}t = 17.5$ and (b) $\Omega_{i0}t = 20$. The separatrices are indicated by the black dashed lines.

We further investigate the formation of electron flow along the separatrix for run 3. According to the guiding center theory, the electron parallel acceleration $\mathrm{d}v_\parallel/\mathrm{d}t$ is given by the following equation:[44]

$$\frac{\mathrm{d}v_\parallel}{\mathrm{d}t} = -\frac{e}{m_\mathrm{e}}E_\parallel - \frac{\mu_\mathrm{e}}{m_\mathrm{e}}\nabla_\parallel B + \boldsymbol{u}_E\frac{\mathrm{d}\hat{\boldsymbol{e}}}{\mathrm{d}t} + o(\varepsilon), \tag{3}$$

where μ_e is the electron magnetic moment, $\boldsymbol{u}_E$ is the $\boldsymbol{E}\times\boldsymbol{B}$ drift velocity, $\hat{\boldsymbol{e}}$ is $\boldsymbol{B}/B$, and $o(\varepsilon)$ represents the small term proportional to m_e/e. If we sum over all electrons in a local region and neglect the small term $o(\varepsilon)$, equation (3) becomes

$$m_\mathrm{e}\frac{\mathrm{d}V_\parallel}{\mathrm{d}t} = -eE_\parallel - \frac{P_\perp}{n_\mathrm{e}B}\nabla_\parallel B + m_\mathrm{e}\boldsymbol{u}_\mathrm{e}\frac{\mathrm{d}\hat{\boldsymbol{e}}}{\mathrm{d}t}, \tag{4}$$

where $V_\parallel$ is the electron parallel bulk velocity summed over the local region, $P_\perp$ is the electron perpendicular pressure, and n_e is the electron number density in the local region. If we assume that the reconnection is in a steady state, equation (4) can be further simplified as

$$m_\mathrm{e}(\boldsymbol{V}\cdot\nabla)V_\parallel = -eE_\parallel - \frac{P_\perp}{n_\mathrm{e}B}\nabla_\parallel B. \tag{5}$$

The left-hand side of Eq. (5) is the convective derivation of electron flow, which is balanced by the parallel electric field force $-eE_\parallel$ and the magnetic mirror force $-P_\perp\nabla_\parallel B/(n_\mathrm{e}B)$ on the right-hand side of Eq. (5).

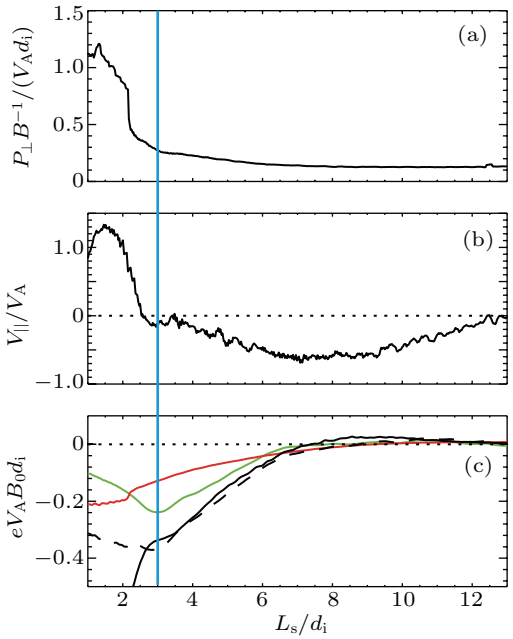


Fig. 7. (a) The profiles of the electron magnetic moment summed over the local region $P_\perp/B$ along the separatrix in the first quadrant at $\Omega_{i0}t = 26.5$. (b) The parallel electron flow velocity $V_\parallel$ along the separatrix in the first quadrant at $\Omega_{i0}t = 26.5$. (c) The integration of parallel electric field force $-\int_{l_0}^{l} eE_\parallel \mathrm{d}l$ (green solid line), magnetic mirror force $-\int_{l_0}^{l} \mathrm{P}_\perp\nabla_\parallel B/(n_\mathrm{e}B)\mathrm{d}l$ (red solid line), the sum $-\int_{l_0}^{l} eE_\parallel + \mathrm{P}_\perp\nabla_\parallel B/(n_\mathrm{e}B)\mathrm{d}l$ (black dashed line), and the electron convective derivation $\int_{l_0}^{l} m_\mathrm{e}(\boldsymbol{V}\cdot\nabla)V_\parallel \mathrm{d}l$ (black solid line) along the separatrix in the first quadrant at $\Omega_{i0}t = 26.5$. In the figure, the distance L_s is measured from the X line along the upper-right separatrix.

Figure 7(a) shows the electron magnetic moment summed over the local region $P_\perp/B$ along the separatrix in the first quadrant at $\Omega_{i0}t = 26.5$ for run 3. The electron parallel bulk velocity $V_\parallel$ along the same separatrix is shown in Fig. 7(b). The integration of parallel electric field force $-\int_{l_0}^{l} eE_\parallel \mathrm{d}l$ (green solid line) along the separatrix in the first quadrant is shown in Fig. 7(c), where l_0 is the end point of the separatrix on the right boundary of the simulation domain. The integration of magnetic mirror force $-\int_{l_0}^{l} \mathrm{P}_\perp\nabla_\parallel B/(n_\mathrm{e}B)\mathrm{d}l$ (red solid line) is also shown in Fig. 7(c). It can be found that from the inflow region to the reconnection X line along the separatrix, both the parallel electric field force and the magnetic

mirror force become more and more important for electron acceleration. If we compare these two mechanisms, the parallel electric field force is more important for electron acceleration; however, the magnetic mirror force cannot be neglected either. In Fig. 7(c), the difference between the electron flow convective derivation $\int_{l_0}^{l} m_e(\boldsymbol{V}\cdot\boldsymbol{\nabla})V_{\parallel}\mathrm{d}l$ (black solid line) and the sum of the parallel electric field force and the magnetic mirror force $-\int_{l_0}^{l} eE_{\parallel}+\mathrm{P}_{\perp}\boldsymbol{\nabla}_{\parallel}B/(n_eB)\mathrm{d}l$ (black dashed line) comes from the nonadiabatic motion of some electrons, which cannot be described by the guiding center theory. This difference becomes much more obvious in the electron diffusion region ($L_s < 3.0d_i$, indicated by the blue solid line in Fig. 7), where the electron motion is decoupled with the local magnetic field and the guiding center theory fails.

We also investigate the influences of the ion-to-electron mass ratio and light speed on the electron depletion layer and parallel electric field in the separatrix region. Figure 8(a) plots the time evolution of the reconnected flux ψ for runs 1–4. A group of runs have the same light speed but different ion-to-electron mass ratios. Obviously, the ion-to-electron mass ratio does not change the reconnection rate, although reconnection occurs earlier with the increase in the mass ratio. Figure 8(b) plots the time evolution of the reconnected flux ψ for runs 3 and 5–7. A group of cases have the same ion-to-electron mass ratio but different light speeds. With the decrease in light speed, reconnection occurs earlier, but the reconnection rate hardly changes.

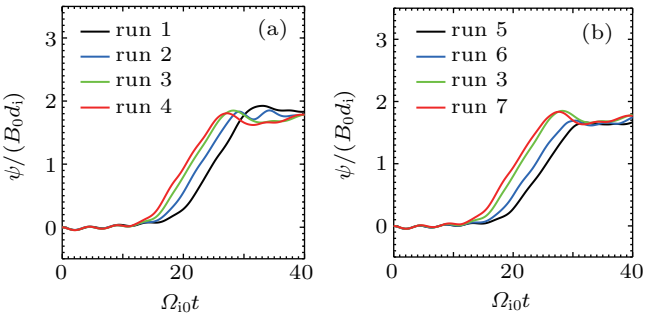


Fig. 8. (a) The time evolution of the reconnected flux ψ for run 1 (black solid line), run 2 (blue solid line), run 3 (green solid line), and run 4 (red solid line). (b) The time evolution of the reconnected flux ψ for run 5 (black solid line), run 6 (blue solid line), run 3 (green solid line), and run 7 (red solid line).

Figures 9(a) and 9(b) show the electron number density n_e and the parallel electron bulk flow velocity $V_{e\parallel}$ along the line at $x = 22.5d_i$, parallel to the z axis for run 1 at $\Omega_{i0}t = 21.25$, run 2 at $\Omega_{i0}t = 19$, run 3 at $\Omega_{i0}t = 17.5$, and run 4 at $\Omega_{i0}t = 16.5$. At these times, the reconnection rates of all runs reach the maximum. With the increase in the mass ratio, the electron depletion layer, as well as the parallel electron bulk flow velocity toward the X line in the separatrix region and away from the X line, become more salient. Figures 10(a) and 10(b) show the electron number density n_e and the parallel electron bulk flow velocity $V_{e\parallel}$ along the line at $x = 22.5d_i$, parallel to the z axis for run 5 at $\Omega_{i0}t = 21$, run 6 at $\Omega_{i0}t = 19.5$, run 3 at $\Omega_{i0}t = 17.5$, and run 7 at $\Omega_{i0}t = 16.75$. The decrease in light speed enhances the electron depletion and parallel flow in the separatrix region.

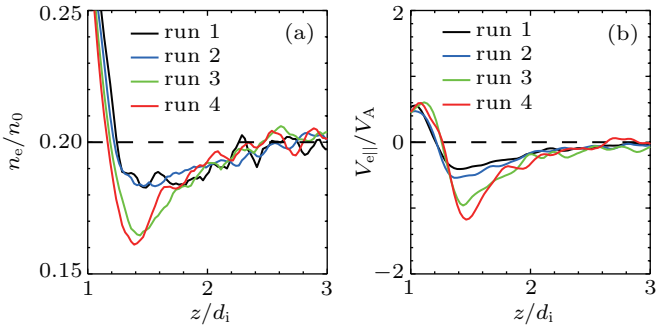


Fig. 9. The profile of (a) the electron number density n_e and (b) the parallel electron bulk flow velocity $V_{e\parallel}$ along the line at $x = 22.5d_i$ parallel to the z axis for run 1 at $\Omega_{i0}t = 21.25$ (black solid lines), run 2 at $\Omega_{i0}t = 19$ (blue solid lines), run 3 at $\Omega_{i0}t = 17.5$ (green solid lines), and run 4 at $\Omega_{i0}t = 16.5$ (red solid lines). The black dashed line in panel (a) indicates the initial electron density in the inflow region $n_b = 0.2n_0$. The black dashed line in panel (b) denotes the value $V_{e\parallel}/v_A = 0$.

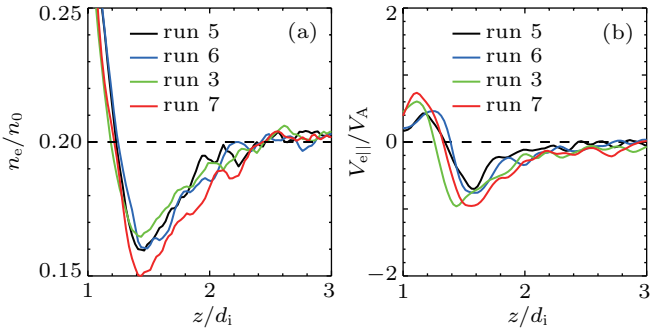


Fig. 10. The profile of (a) the electron number density n_e and (b) the parallel electron bulk flow velocity $V_{e\parallel}$ along the line at $x = 22.5d_i$ parallel to the z axis for run 5 at $\Omega_{i0}t = 21$ (black solid lines), run 6 at $\Omega_{i0}t = 19.5$ (blue solid lines), run 3 at $\Omega_{i0}t = 17.5$ (green solid lines), and run 7 at $\Omega_{i0}t = 16.75$ (red solid lines). The black dashed line in panel (a) indicates the initial electron density in the inflow region $n_b = 0.2n_0$. The black dashed line in panel (b) denotes the value $V_{e\parallel}/v_A = 0$.

Figure 11(a) shows the parallel electrostatic potential $\Phi_{\parallel}$ along the separatrix for run 1 at $\Omega_{i0}t = 21.25$, run 2 at $\Omega_{i0}t = 19$, run 3 at $\Omega_{i0}t = 17.5$, and run 4 at $\Omega_{i0}t = 16.5$. At these times, all runs obtain the maximum reconnection rate. It can be found that with the increase in the mass ratio, the parallel electrostatic potential $\Phi_{\parallel}$ along the separatrix is enhanced. Figure 11(b) shows the $\Phi_{\parallel}$ along the separatrix for run 5 at $\Omega_{i0}t = 21$, run 6 at $\Omega_{i0}t = 19.5$, run 3 at $\Omega_{i0}t = 17.5$, and run 7 at $\Omega_{i0}t = 16.75$. At these times, all runs obtain the maximum reconnection rate. With the decrease in light speed, the parallel electrostatic potential in the separatrix region also tends to be more salient.

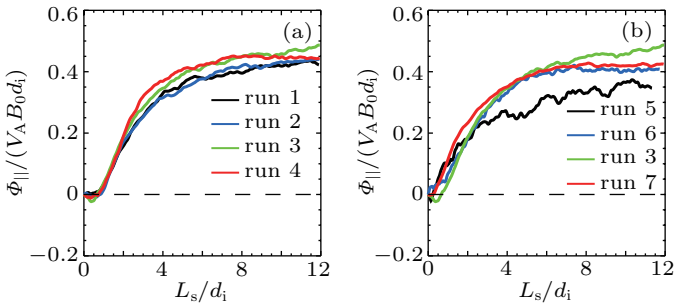


Fig. 11. (a) The parallel electrostatic potential $\Phi_{\parallel}$ along the separatrix for run 1 at $\Omega_{i0}t = 21.25$ (black solid line), run 2 at $\Omega_{i0}t = 19$ (blue solid line), run 3 at $\Omega_{i0}t = 17.5$ (green solid line), and run 4 at $\Omega_{i0}t = 16.5$ (red solid line). (b) The parallel electrostatic potential $\Phi_{\parallel}$ along the separatrix for run 5 at $\Omega_{i0}t = 21$ (red solid line), run 6 at $\Omega_{i0}t = 19.5$ (blue solid line), run 3 at $\Omega_{i0}t = 17.5$ (green solid line), and run 7 at $\Omega_{i0}t = 16.75$ (red solid line). In the figure, the black dashed lines denote the value $\Phi_{\parallel}/v_A B_0 d_i = 0$.

4. Summary and discussion

In this paper, with 2D PIC simulations, we studied the properties of the electron depletion layer and parallel electric field in the separatrix region during anti-parallel reconnection. At first, the parallel electric field pointing away from the X line is formed in the separatrix region, and then the parallel electric field pointing toward the X line is developed in the separatrix region around the X line. Both the increase in the ion-to electron mass ratio and decrease in light speed make the electron depletion layer and parallel electric field more salient in the separatrix region.

Satellite observations have already revealed the existence of the parallel electric field in the separatrix region during magnetic reconnection.[17,45,46] Both observations and our simulations have shown that in addition to the reconnection electric field induced around the X line, there still exists the parallel electric field in the separatrix region, which may play an important role in electron acceleration during magnetic reconnection. How the parallel electric field in the separatrix region will act on electron acceleration during magnetic reconnection is a direction for our future work.

References

[1] Vasyliunas V M 1975 *Rev. Geophys.* **13** 303
[2] Biskamp D 2000 *Magnetic Reconnection in Plasma* (Cambridge: Cambridge University Press)
[3] Priest E and Forbes T 2000 *Magnetic Reconnection: MHD Theory and Applications* (Cambridge: Cambridge University Press)
[4] Daughton W, Scudder J and Karimabadi H 2006 *Phys. Plasmas* **13** 072101
[5] Lu S, Lu Q, Huang C and Wang S 2013 *Phys. Plasmas* **20** 061203
[6] Zhou M, Ashour-Abdalla M, Deng X, Pang Y, Fu H, Walker R, Lapenta G, Huang S, Xu X and Tang R 2017 *J. Geophys. Res.* **122** 9513
[7] Hoshino M, Mukai T, Terasawa T and Shinohara I 2001 *J. Geophys. Res.* **106** 25979
[8] Fu X, Lu Q and Wang S 2006 *Phys. Plasmas* **13** 012309
[9] Huang C, Lu Q and Wang S 2010 *Phys. Plasmas* **17** 072306
[10] Huang S, Vaivads A, Khotyaintsev Y V, Zhou M, Fu H, Retinò A, Deng X, Andre M, Cully C M, He J, Sahraoui F, Yuan Z and Pang Y 2012 *Geophys. Rev. Lett.* **39** L11103
[11] Fu H, Khotyaintsev Y V, Vaivads A, Retinò A and André M 2013 *Nat. Phys.* **9** 426
[12] Dahlin J, Drake J and Swisdak M 2014 *Phys. Plasmas* **21** 092304
[13] Wang H, Lu Q, Huang C and Wang S 2016 *Astrophys. J.* **821** 84
[14] Lu S, Angelopoulos V and Fu H 2016 *J. Geophys. Res.* **121** 9483
[15] Lu Q, Wang H, Huang K, Wang R and Wang S 2018 *Phys. Plasmas* **25** 072126
[16] Zhou M, El-Alaoui M, Lapenta G, Berchem J, Richard R L, Schriver D and Walker R J 2018 *J. Geophys. Res.* **123** 8087
[17] Wang R, Lu Q, Khotyaintsev Y V, Volwerk M, Du A, Nakamura R, Gonzalez W D, Sun X, Baumjohann W, Li X, Zhang T, Fazakerley A N, Huang C and Wu M 2014 *Geophys. Res. Lett.* **41** 4851
[18] Lu Q, Huang C, Xie J, Wang R, Wu M, Vaivads A and Wang S 2010 *J. Geophys. Res.* **115** A11208
[19] Lu S, Lu Q, Cao Y, Huang C, Xie J and Wang S 2011 *Chin. Sci. Bull.* **56** 48
[20] Wang R, Du A, Nakamura R, Lu Q, Khotyaintsev Y V, Volwerk M, Zhang T, Kronberg E A, Daly P W and Fazakerley A N 2013 *Geophys. Res. Lett.* **40** 1
[21] Egedal J, Le A and Daughton W 2013 *Phys. Plasmas* **20** 061201
[22] Huang C, Lu Q, Wang P, Wu M and Wang S 2014 *J. Geophys. Res.* **119** 6445
[23] Lapenta G, Markidis S, Divin A, Newman D and Goldman M 2015 *Phys. Plasmas* **81** 325810109
[24] Egedal J, Le A, Daughton W, Wetherton B, Cassak P A, Chen L, Lavraud B, Torbert R B, Dorelli J, Gershman D J and Avanov L A 2016 *Phys. Rev. Lett.* **117** 185101
[25] Birn J, Drake J F, Shay M A, Rogers B N, Denton R E, Hesse M, Kuznetsova M, Ma Z, Bhattacharjee A, Otto A and Pritchett P L 2001 *J. Geophys. Res.* **106** 3715
[26] Pritchett P 2001 *J. Geophys. Res.* **106** 3783
[27] Nagai T, Shinohara I, Fujimoto M, Machida S, Nakamura R, Saito Y and Mukai T 2003 *J. Geophys. Res.* **108** 1357
[28] Sonnerup B 1979 *Space Plasma Physics* (Vol. 3) (Kennel C F, Lanzerotti L J and Parker E N, Ed.) (Amsterdam: North-Holland Publishing) p. 46
[29] Terasawa T 1983 *Geophys. Res. Lett.* **10** 475
[30] Hesse M, Birn J and Kuznetsova M 2001 *J. Geophys. Res.* **106** 3721
[31] Shay M A, Drake J F, Rogers B N and Denton R E 2001 *J. Geophys. Res.* **106** 3759
[32] Lai X, Zhou M, Deng X, Li T and Huang S 2015 *Chin. Phys. Lett.* **32** 095202
[33] Wang R, Nakamura R, Lu Q, Baumjohann W, Ergun R E, Burch J L, Volwerk M, Varsani A, Nakamura T, Gonzalez W, Giles B, Gershman D and Wang S 2017 *Phys. Rev. Lett.* **118** 175101
[34] Yang H, Jin S and Zhou G 2006 *J. Geophys. Res.* **111** A11223
[35] Ma Z and Fend S 2008 *Chin. Phys. Lett.* **25** 2934
[36] Bessho N, Chen L, Germaschewski K and Bhattacharjee A 2015 *J. Geophys. Res. Space Phys.* **120** 9355
[37] Mozer F S, Bale S D and Phan T D 2002 *Phys. Rev. Lett.* **89** 015002
[38] Lu S, Lu Q, Shao X, Yoon P H and Wang S 2011 *Phys. Plasmas* **18** 072105
[39] Lu S, Lu Q, Dong Q, Huang C, Wang S, Zhu J, Sheng Z and Zhang J 2013 *Phys. Plasmas* **20** 112110
[40] Huang C, Lu Q, Guo F, Wu M, Du A and Wang S 2015 *Geophys. Res. Lett.* **42** 7282
[41] Huang K, Lu Q, Huang C, Dong Q, Wang H, Fan F, Sheng Z, Wang S and Zhang J 2017 *Phys. Plasmas* **24** 102101
[42] Wang P, Huang C, Lu Q, Wang R and Wang S 2013 *Chin. Phys. Lett.* **30** 125202
[43] Zhang Z, Lu Q, Dong Q, Lu S, Huang C, Wu M, Sheng Z, Wang S and Zhang J 2013 *Chin. Phys. Lett.* **30** 045201
[44] Northrop T 1963 *The Adiabatic Motion of Charged Particles* (New York: Wiley)
[45] Retinò A, Vaivads A, André M, Saharaoui F, Khotyaintsev Y, Pickett J S, Bavassano-Cattaneo M B, Marcucci M F, Morooka M, Owen J C, Buchert S C and Cornilleau-Wehrlin N 2006 *Geophys. Res. Lett.* **33** L06101
[46] Lindstedt T, Khotyaintsev Y V, Vaivads A, André M, Fear R C, Lavraud B, Haaland S and Owen C J 2009 *Ann. Geophys.* **27** 4039